# Implementation of Different RF-Chains to Drive Acousto-Optical Tunable Filters in the Framework of an ESA Space Mission

***J. Vanhamel[1], S. Berkenbosch[1], E. Dekemper[2], D. Fussen[2], P. Leroux[3], E. Neefs[1], and E. Van Lil[4]***

[1]Engineering Department
Royal Belgian Institute for Space Aeronomy Ringlaan 3, 1180 Brussels, Belgium
E-mail: jurgen.vanhamel@aeronomie.be

[2]Department of Solar Radiation in Atmospheres Royal Belgian Institute for Space Aeronomy
Ringlaan 3, 1180 Brussels, Belgium

[3]KU Leuven, Department of Electrical Engineering ESAT, Advanced Integrated Sensing Lab (AdvISe)
Kleinhoefstraat 4, 2440 Geel, Belgium

[4]KU Leuven, Department of Electrical Engineering ESAT – TELEMIC, Telecommunications and Microwaves
Kasteelpark Arenberg 10, bus 244, 3001 Leuven, Belgium
E-mail: streltsa@erau.edu

## Abstract

The work reported in this paper addresses different solutions to the problem of building a space-qualified RF chain for an acousto-optical tunable filter. This research was undertaken as part of the development of the ALTIUS space mission (atmospheric limb tracker for the investigation of the upcoming stratosphere), which aims at the measurement of atmospheric trace species (ozone, nitrogen dioxide, methane, water vapor,...) concentration profiles with a high spatial resolution.

## 1. Introduction

Wide-aperture acousto-optical tunable filters (AOTF) appeared in the 1970s [1] and found applications in various areas, such as agriculture (crop-stress monitoring), the food industry (product quality), biology (fluorescence spectroscopy), etc. Their main advantages are robustness, compactness, low power consumption, high filtering efficiency, ability to be tuned, potentially high spectral resolution ($< 1$ nm), and good image quality. In general, they offer interesting features for meeting the needs in hyperspectral-imaging applications.

The physical process behind the wide-aperture acousto-optical tunable filter is the interaction of light and sound inside a birefringent crystal. For a given acoustic frequency, only photons of a particular energy (i.e., wavelength) will couple with the acoustic wave, and then leave the crystal in a slightly different direction than the rest of the light. By focusing the diverted beam onto a detector, one effectively performs a spectral image of the scene. Selecting another window of the light spectrum only requires the tuning of the sound frequency. A piezoelectric transducer bonded to the crystal is responsible for converting the electrical RF signal into an acoustic wave.

As most acousto-optical tunable filters operating in the visible and near-infrared domains are driven with frequencies ranging from a few MHz to several hundreds of MHz, they do not necessitate particular electronics equipment. This statement does not hold when it comes to operating acousto-optical tunable filters in a space environment: the RF-driving chain must be made from the limited catalogue of space-qualified parts. The problem gets even larger when frequencies of several tens of MHz or higher must be generated.

The work reported in this paper addresses different solutions to the problem of building a space-qualified RF-

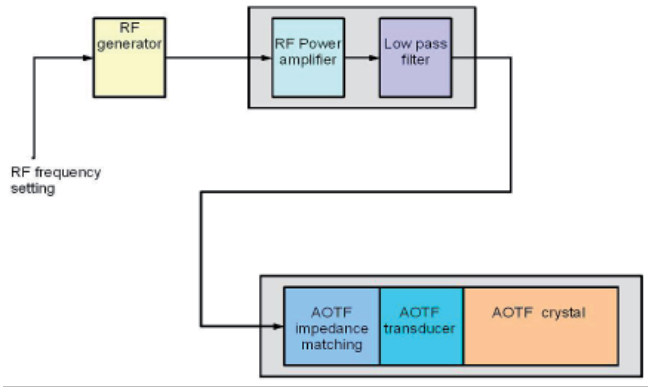


**Figure 1. The channel RF-chain concept.**

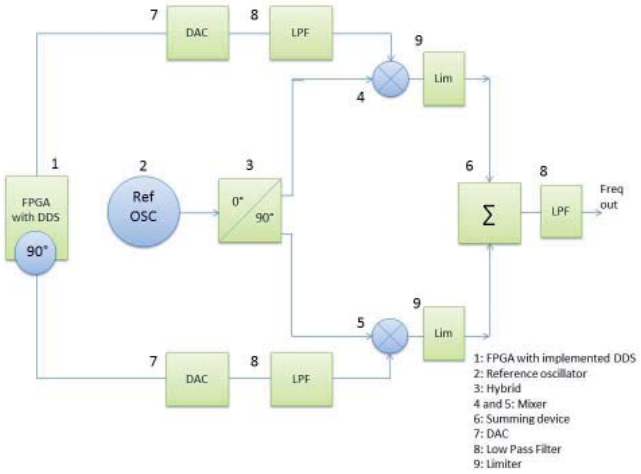


**Figure 2. The Hilbert-transform solution setup.**

chain for an acousto-optical tunable filter. This research was undertaken as part of the development of the ALTIUS space mission (atmospheric limb tracker for the investigation of the upcoming stratosphere), which aims at the measurement of atmospheric trace species (ozone, nitrogen dioxide, methane, water vapor,...) concentration profiles with a high spatial resolution [2, 3]. The measurement concept relies on the acquisition of spectral images of the bright atmospheric limb at well-chosen wavelengths. The imager concept allows avoiding the need for scanning the atmosphere, as was done by previous remote-sensing missions. The instrument will be mounted onboard a PROBA satellite (Project for On-Board Autonomy) [4-6]. The PROBA-satellite is a platform containing all the essential subsystems, such as a GPS, an attitude and orbit control system, etc., to facilitate the payload, which is placed on top of the platform. The complete project (platform and payload) is being developed under the supervision of ESA (European Space Agency), and with funding from the Belgian Science Policy Office (BELSPO).

The original ALTIUS concept made use of three independent spectral imagers (channels), each of them relying on an acousto-optical tunable filter capable of isolating narrow pass-bands across the channel's spectral range (ultraviolet, UV, from 250 nm to 400 nm; visible, from 440 nm to 800 nm; near-infrared, NIR, from 900 nm to 1800 nm). For the visible and NIR channels, the two acousto-optical tunable filters will be made of a paratellurite crystal. For the UV channel, the acousto-optical tunable filter would have been made from a KDP crystal (potassium dihydrogen phosphate). Unfortunately, the latter did not reach the necessary level of maturity for a space mission, and the KDP-based acousto-optical tunable filter was replaced by a stack of Fabry-Pérot interferometers (FPI). Nevertheless, for technological interest, the acousto-optical tunable filter approach will also be developed and matured for the UV-channel up to flight level.

The focus of this paper was to design, for each of the different channels, a dedicated RF-chain containing an RF generator and an RF amplifier (see Figure 1). The output of the RF amplifier was tunable to a specific frequency and a specific power level, and was injected into the acousto-optical tunable filter's transducer via an impedance-matching network.

Different architectures [7-11] are possible to generate the frequency range needed for the different wavelength domains. While the Hilbert-transform solution will be only summarized here and not further investigated, this paper focuses on the phase-locked loop (PLL) solution. Phased-locked loop solutions were bread-boarded for the three wavelength domains. A detailed study was done on the achievable power levels in the infrared, visible, and the ultraviolet.

**Table 1. The available preliminary design requirements.**

| Requirement | Value |
|---|---|
| Unwanted spectral components in RF output | < –30 dBc |
| UV channel frequency range | 130 - 260 MHz |
| Visible channel frequency range | 60 - 120 MHz |
| NIR channel frequency range | 30 - 60 MHz |
| Nominal load | 50 Ohms |
| RF generator dc power consumption | < 2 W |
| RF generator output power level | > 0 dBm |

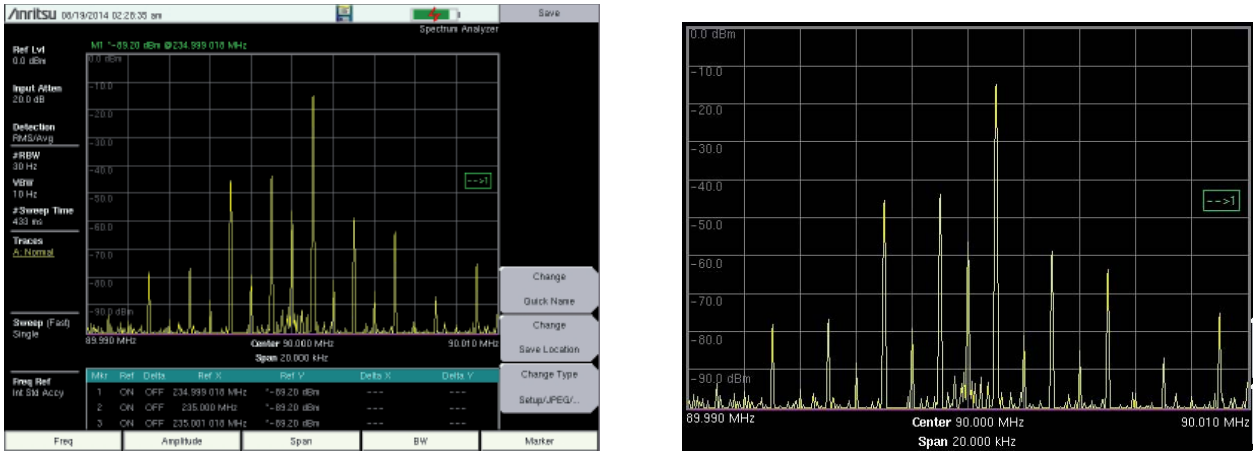


**Figure 3. The spectral output for the visible channel.**

## 2. RF Generator Architectures

Both the RF generator and the RF amplifier will have specific requirements for electrical performance, sensitivity, frequency range, and resolution. Their development will focus on survivability in space and compliance with the selected spacecraft. For this, a well-defined package of environmental tests has to be carried out, such as thermal-vacuum, radiation, vibration, shock, and EMC (electromagnetic compatibility). The test levels were derived from the scientific requirements for the instrument. Because the project is currently in a preliminary design phase, some requirements still need to be defined. For instance, the choice of the launcher will determine several environmental parameters. This paper will focus on fulfilling of the requirements listed in Table 1.

All the other requirements will be determined in a later stage. To fulfill the environmental requirements, the electronic components need to be selected and built in accordance with "space-qualified" standards. Because of the space environment wherein this instrument has to perform, the availability of electronic components is limited to those screened and qualified for space applications. ESA also restricts the use of components to those present in their preferred parts list. This restricts the possibilities for generating an RF signal based on a high-tech up-to-date solution. Solutions containing commercial electronics also cannot be retained.

For the design of a space-qualified acousto-optical tunable-filter RF generator, different approaches were investigated [7-11]. Taking into account the space environment, and the limitations of restricted power, voltage levels, mass, and volume, two solutions were considered, namely the Hilbert transform [8, 9] and the phased-locked-loop approach [10, 11]. Today, the latter solution is preferred, and hence was further investigated in this paper. This is because it has better spectral purity, lower complexity, lower power consumption, and a higher output-power level. A scientific space project under the supervision of ESA in a preliminary design phase needs to have a main and a spare solution. This is why the Hilbert transform was kept as a backup. The setup is explained in Figure 2.

The key elements in the Hilbert-transform solution are a fixed oscillator and an FPGA (field-programmable gate array) from Actel-Microsemi (RTAX2000S-CQ352V) [12]. In the FPGA, a firmware DDS (direct digital synthesizer) was implemented that created two 90°-shifted digital waveforms. The output of the FPGA was presented to two DACs (digital-to-analog converters) [13] that converted the output into analog sine waves. The signals in both chains are then filtered by an LPF (low-pass filter) and applied to two mixers. The output of a reference oscillator was shifted by 0° and 90°. Each output was combined in a mixer stage and filtered (low-pass filter). Both chains were summed in a summing device. This sine wave was filtered before entered the RF amplifier. Several breadboards were built and tested for the different channels. Looking at the spectral output – for example, of the visible channel – it

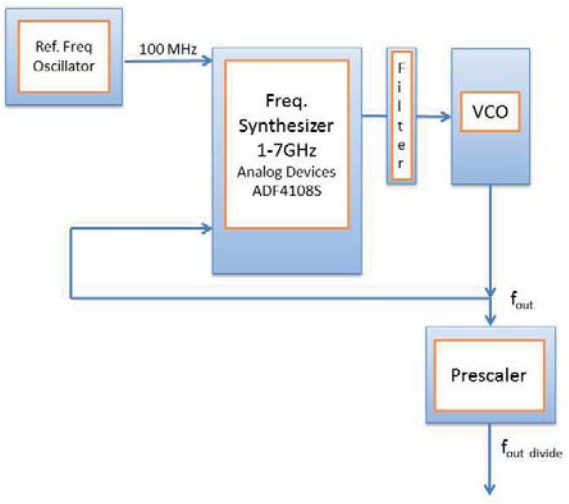


**Figure 4. The phase-locked-loop solution setup.**

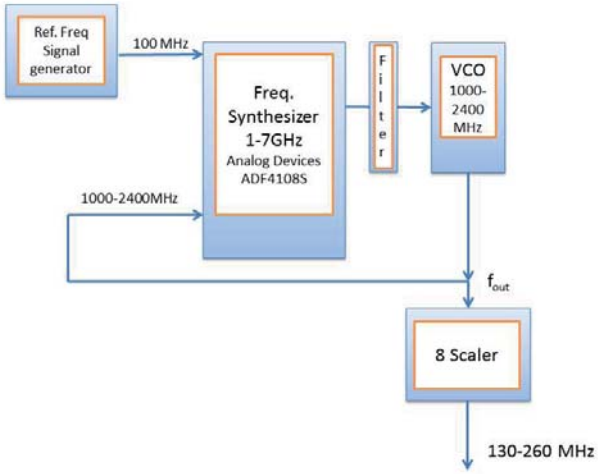


**Figure 5. The UV-channel setup.**

could be seen that many harmonics and spurs were created, depending on the frequency used (Figure 3). The production of the harmonics and spurs was caused by several mixing stages in the setup, as well as the summing at the end of the chain. The level of the spurs and harmonics was still below the requirement of −30 dBc.

Although all requirements concerning harmonic suppression and output level were fulfilled, and although all proposed components existed in a space-qualified version, the solution exceeded the available electrical-power budget. The higher mass, volume, and complexity also made it less attractive compared to the phased-locked-loop solution. The reason was that the Hilbert transform used an FPGA (1 W) and two mixer stages. These mixers were passive devices, which meant that the input power had to be high (around +7 dBm). For the Hilbert transform, two extra DACs would have been needed, which implied an additional 2 × 660 mW. Together with the lower output level of the RF generator (compare Figure 3 with Figures 6, 9, and 12), this would have resulted in twice the needed dc power compared to the phased-locked-loop solution.

The phased-locked-loop design (Figure 4) used an ADF4108S space-qualified frequency synthesizer from Analog Devices [14], a voltage-controlled oscillator (VCO), an active-loop filter, and a space-qualified prescaler from Peregrine Semiconductor. The power consumption of this setup was limited compared to the Hilbert-transform solution. The ADF4108S consumed around 100 mW, the VCO consumed around 200 mW, and the prescaler consumed around 40 mW. An FPGA was also needed to steer the RF chain, which introduced an extra power consumption of 1 W. While the power consumption for the Hilbert-transform solution was estimated to be 3 W, the estimated power consumption of the phased-locked-loop solution was 1.5 W. Depending on the channel setup, and taking into account some margins, the total power varied from one channel to another: UV: ±1400 mW; visible: ±1450 mW; and NIR: ±1450 mW. An additional advantage of the phased-locked loop was the increased output level of the signal.

In the next paragraphs, the detailed phased-locked-loop design for the different channels is described, and the test results obtained on the breadboards are explained.

## 3. Test Results

### 3.1 The UV Channel

For the UV channel (Figure 5), the ADF4108S from Analog Devices was used together with an in-house custom-designed active-loop filter. In the phased-locked-loop a VCO (Mini-Circuits ZX95-2500W+) [15] was used, which was controlled between 1 GHz and 2.4 GHz, followed by a divide-by-eight prescaler from Peregrine Semiconductor [16].

This phased-locked-loop combination allowed spanning the required output-frequency range for the UV channel (130 MHz to 260 MHz). Tests showed that the generated spectrum was compliant with the requirements: no excessive harmonics or spurs existed in the spectrum

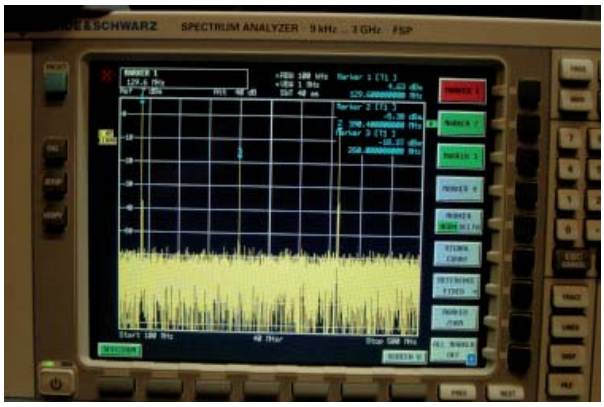

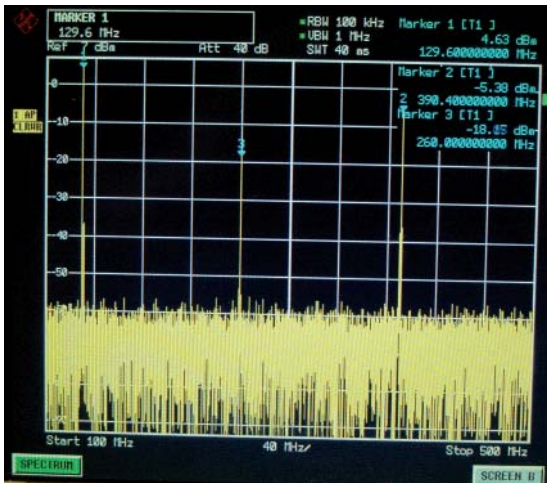


**Figure 6. The output signal at 129.6 MHz after the divide-by-eight prescaler.**

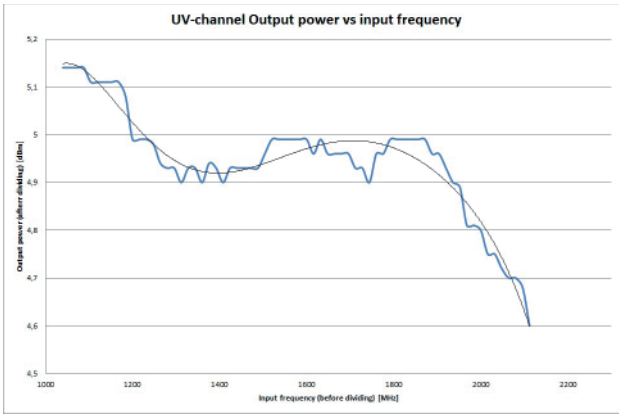


**Figure 7. The output power level of the UV channel.**

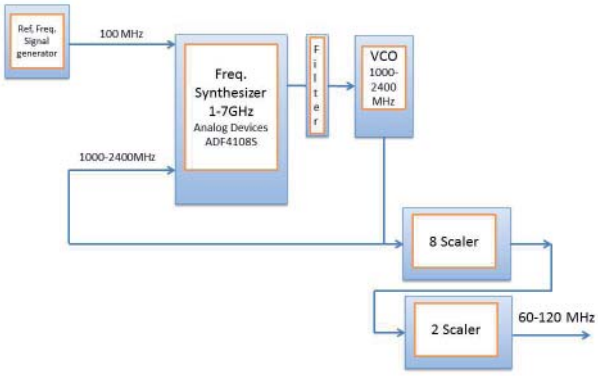


**Figure 8. The visible-channel setup.**

(Figure 6), the second harmonic was less than −22 dBc, and the third harmonic was −10 dBc. The use of an additional passive third-order bandpass hourglass filter that had a bandwidth of 130 MHz and a center frequency of 195 MHz suppressed these higher harmonics. As a consequence, the power level of the output signal was attenuated by 10 dB because of this filter.

Additionally, tests were carried out to check the output level of the RF generator (Figure 5). Different input frequencies were programmed into the ADF4108, delivering output frequencies in the desired range. The VCO's output level varied with the output frequency. The lowest output level was around −1.4 dBm, and the highest output was around +4.3 dBm. These numbers were based on the datasheets of the VCO used. A fit with a sixth-order polynomial indicated the trend of the setup's output-power curve (Figure 7). The drift of the output-power level was quite limited in the frequency range. At the low end, the output power was around 5.1 dBm, and at the higher end, the power was around 4.6 dBm, resulting in a spread of around 0.5 dB.

## 3.2 The Visible Channel

The same ADF4108, Mini-Circuits VCO, and custom-made loop filter were used for the RF generator of the visible channel (Figure 8). However, a different divider combination was used with divide-by-eight and divide-by-two prescalers [17] to match the required frequency range (60 MHz to 120 MHz), because no space-qualified divide-by-16 prescaler was available on the market today.

As for the RF generator in the UV channel, the VCO output could also be controlled in the range of 1 GHz to 2.4 GHz. At the lower end of the required range (with the synthesizer frequency set to 1 GHz), an output frequency of 62.6 MHz was obtained after the prescalers with harmonics located at 187.9 MHz (−9.7 dBc) and 313.2 MHz (−14.5 dBc) (Figure 9). Again, no excessive harmonics or spurs existed in the spectrum. The requirement of −30 dBc could easily be met by implementing a passive third-order bandpass hourglass filter. The upper end of the required output frequency range could be reached with a synthesizer

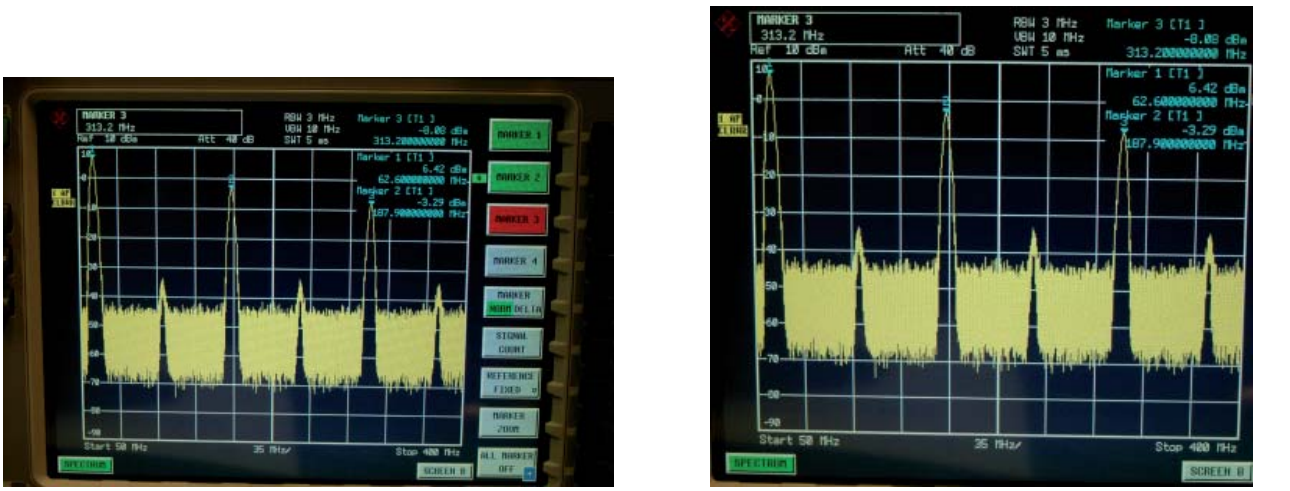

**Figure 9. The output signal at 62.5 MHz after the divide-by-eight and divide-by-two prescalers.**

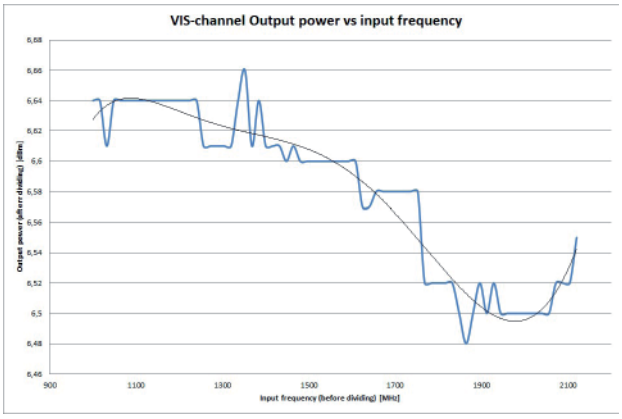


**Figure 10. The output power level of the visible channel.**

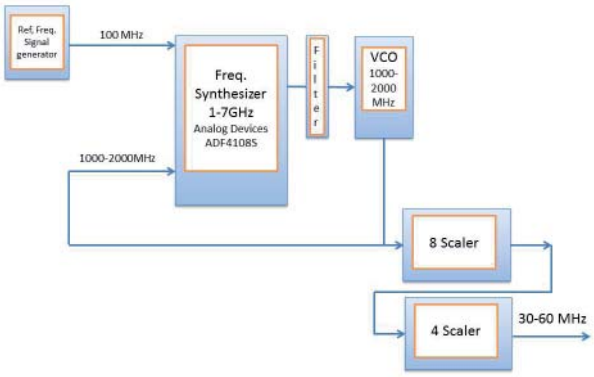


**Figure 11. The NIR-channel setup.**

frequency of 1.92 GHz, after scaling leading to an output frequency of 120 MHz. Additional filtering, similar to that used in the UV channel, removed the harmonics from the output.

Similarly to the UV channel, the stability of the output level was verified (Figure 10). At the low end of the frequency range, the output power was around 6.7 dBm, and it was around 6.5 dBm at the higher end, giving a spread of about 0.15 dB. Based on these numbers, it could be concluded that the stability of the RF generator was proven.

## 3.3 The NIR Channel

The phased-locked-loop solution for the NIR channel was very similar to the two previous designs (Figure 11). The same components were used. The VCO was used in a slightly reduced frequency range, while the end stage was composed of a divide-by-eight followed by a divide-by-four prescaler [18]. No space-qualified divide-by-32 prescaler exists on the market today. With this setup, an output frequency range between 30 MHz and 60 MHz was obtained.

The output of the VCO was controlled between 1 GHz and 2 GHz. At a synthesizer frequency of 1.23 GHz, an output frequency of 38.439 MHz was obtained after the prescaler stage, with harmonics at 115.32 MHz ( –9.8 dBc) and 192.54 MHz ( –14.1 dBc) (Figure 12), well below the expected –30 dBc if a passive third-order bandpass hourglass filter was used.

Figure 13 shows the deviation of the output power for the measurements performed. At the low end of the frequency range, the output power was around 6.0 dBm. At the high end, it was around 5.8 dBm, yielding a spread of about 0.2 dB.

## 4. Conclusions and Future Work

This study was part of the development of the driving electronics of a spaceborne remote-sensing instrument (ALTIUS), which used acousto-optical tunable filters to take spectral images of the bright atmospheric limb in order to retrieve the concentration profiles of key trace species. Although building RF-chains for driving acousto-optical tunable filters on the ground is a common task, it required

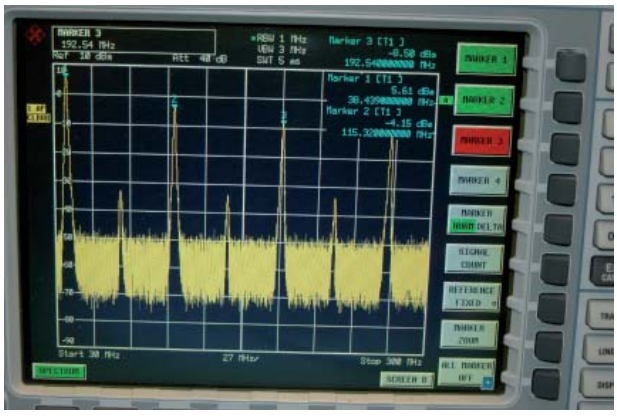

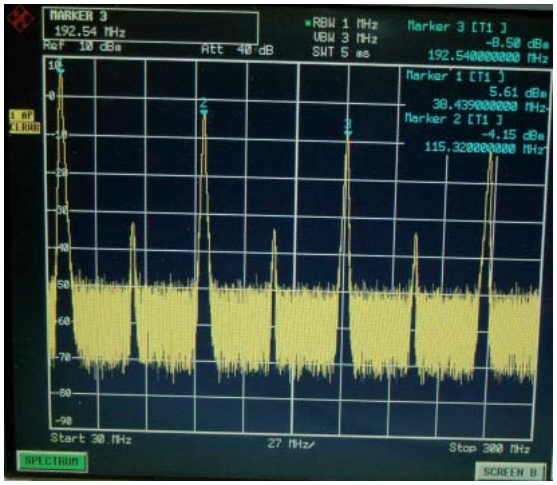


**Figure 12. The output signal at 38.439 MHz after the divide-by-eight and divide-by-four prescalers.**

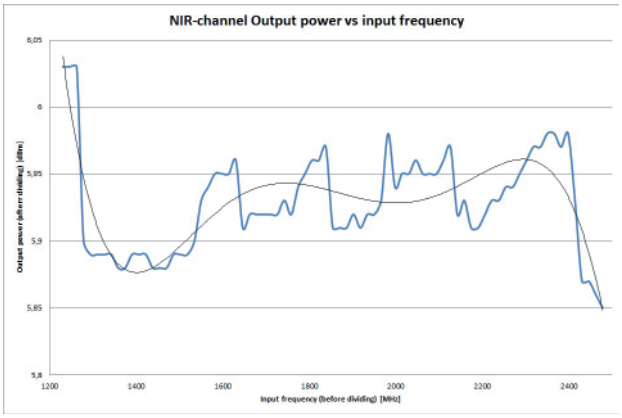


**Figure 13. The output power level of the NIR channel.**

specific developments in the framework of a space instrument, as it had to undergo space-qualification procedures. Two driving concepts were designed and bread-boarded.

As a conclusion of this work, it was clear that for the generation of the RF signals driving the three acousto-optical tunable filters originally proposed in the ALTIUS concept, a phased-locked-loop solution was preferred over a Hilbert-transform solution. A phased-locked-loop setup offered less complexity (fewer parts needed), and hence a reduced printed-circuit-board area, reduced mass, and better resistance to mechanical stresses. The implementation of the design into a flight-compatible form, rather than a breadboard, and with realistic harnessing and connectors is ongoing.

The achieved output levels for the phased-locked-loop solution showed acceptable output-level stabilities in the applied frequency range of 0.2 dB in the NIR and visible channels, and 0.5 dB in the UV channel. Both values were in line with the input specifications of the RF amplifiers. It was shown that the use of a combination of prescalers (visible and NIR channels) in the last stage instead of a single prescaler had no negative impact on the stability.

Future work will consist of assessing the stability of the output signal, including the thermally induced jitter. It is known that the performance of analog VCO circuits has to be strictly monitored (and sometimes even controlled) in environments with thermal variations. Further investigation will clarify these items.

## 5. Acknowledgments

The ALTIUS project is supported by the Belgian Federal Science Policy Office (BELSPO), and funded through ESA-PRODEX contract PEA4200090274.

## 6. References

1. I. C. Change, "Noncollinear Acousto-Optic Filter with Large Angular Aperture," *Applied Physics Letters*, **25**, 1974, pp. 370-372.

2. E. Dekemper, D. Fussen, B. Van Opstal, J. Vanhamel, D. Pieroux, F. Vanhellemont, N. Mateshvili, G. Franssens, V. Voloshinov, C. Janssen, and H. Elandaloussi, "ALTIUS: A Spaceborne AOTF-Based UV-VIS-NIR Hyperspectral Imager for Atmospheric Remote Sensing," *Proceedings of SPIE*, **9241-92410L**, 1-10, 2014.

3. E. Dekemper, D. Fussen, F. Vanhellemont, D. Pieroux, N. Mateshvili, G. Franssens, Q. Errera, J. Vanhamel, E. Neefs, L. De Vos, and L. Aballea, "ALTIUS, A Future Small Mission for $O_3$ and Other Atmospheric Trace Species Concentration Profiles Retrieval," *Geophysical Research Abstracts*, **18**, EGU2016-17653, 2016.

4. K. Gantois, S. Santandrea, F. Teston, K. Strauch, J. Zender, E. Tilmans, and D. Gerrits, "ESA's Second In-Orbit Technology Demonstration Mission: Proba-2," *ESA Bulletin-European Space Agency*, **144**, November 2010, pp. 22-33.

5. M. J. Barnsley, J. J. Settle, M. A. Cutter, D. R. Lobb, and F. Teston, "The PROBA/CHRIS Mission: A Low-Cost Smallsat for Hyperspectral Multiangle Observations of the Earth Surface and Atmosphere," *IEEE Transactions on Geoscience and Remote Sensing*, **42**, 7, July 2004, pp. 1512-1520.

6. F. Teston, P. Vuilleumier, D. Hardy, E. Tilmans, and K. Gantois, "Proba Proves the Technology," *ESA Bulletin-European Space Agency*, **129**, February 2007, pp. 47-53.

7. J. Vanhamel, D. Fussen, E. Dekemper, E . Neefs, B. Vanopstal, D. Pieroux, J. Maes, E. Van Lil, and P. Leroux, "RF-Driving of Acoustic-Optical Tunable Filters; Design, Realization and Qualification of Analog and Digital Modules for ESA," *Microelectronics Reliability*, **55**, 2015, pp. 2103-2107.

8. P. Das, D. Shklarsky and L. B. Milstein, "SAW Implemented Real-Time Hilbert Transform and its Application in SSB," IEEE Ultrasonics Symposium, 1979, pp. 752-756

9. L. Moura and P. Monteiro. "Design Method for FIR-Based Hilbert Transform Filters Suitable for Broadband AM-SSB," *Electronics Letters*, **38**, 12, June 6, 2002, pp. 605-606.

10. I. A. Young, J. K. Greason, and K. L. Wong, "A PLL Clock Generator with 5 to 110 MHz of Lock Range for Microprocessors," *IEEE Journal of Solid State Circuits*, 1992, pp. 1599-1607.

11. R.E. Best, *Phase-Locked Loops, Sixth Edition*, New York, McGraw-Hill, USA, 2007.

12. The Actel RTAX FPGA, RTAX2000S-CQ352V (V-flow) www.microsemi.com/products/fpga-soc/radtolerant-fpgas/rtax-s-sl

13. Texas Instruments Digital to Analog Converter DAC5675 A-SP, www.ti.com/product/dac5675a

14. Information and datasheet for the Analog Devices frequency synthesizer (1-7 GHz) ADF4180S, www.analog.com/en/products/application-specific/militaryaerospace/aerospace/adf4108s.html

15. Information and datasheet for the VCO of Mini-Circuits (ZX95-2500W+), http://194.75.38.69/pdfs/ZX95-2500W+.pdf

16. Information and datasheet for the Peregrine 8 prescaler PE9303, www.psemi.com/products/prescalers/pe9303

17. Information and datasheet for the Peregrine 2 prescaler PE9311, www.psemi.com/products/prescalers/pe9311

18. Information and datasheet for the Peregrine 4 prescaler PE9312, www.psemi.com/products/prescalers/pe9312